# One-Dimensional Oxalato-Bridged Metal(II) Complexes with 4-Amino-1,2,4-triazole as Apical Ligand

**Urko García-Couceiro,[a] Oscar Castillo,*[a] Antonio Luque,*[a] Juan P. García-Terán,[a] Garikoitz Beobide,[a] and Pascual Román[a]**

**Keywords:** Chain structures / Oxalato bridging ligand / Triazole / X-ray diffraction / Structure–magnetism relationships

The synthesis, chemical characterization, thermal behavior and magnetic properties of six new one-dimensional oxalato-bridged metal(II) complexes of formula $[M(\mu\text{-ox})(4atr)_2]_n$ [$M^{II}$ = Cu (**1**), Ni (**2**), Co (**3**), Zn (**4**), Fe(**5**)] and $[Cd(\mu\text{-ox})(4atr)_2(H_2O)]_n$ (**6**) (ox = oxalato dianion, 4atr = 4-amino-1,2,4-triazole) are reported. The crystal structures of **1** and **6** have been solved by single-crystal X-ray diffraction, whereas the remaining compounds have been studied by means of X-ray powder diffraction methods. Compounds **1**–**5** are isomorphous and crystallize in the triclinic space group $P\bar{1}$ with unit cell parameters for **1** of $a$ = 5.538(1) Å, $b$ = 7.663(1) Å, $c$ = 7.711(2) Å, $\alpha$ = 62.21(1)°, $\beta$ = 73.91(1)°, $\gamma$ = 86.11(1)°, and $Z$ = 1. The crystal structures are comprised of one-dimensional linear chains in which the *trans*-$[M(4atr)_2]^{2+}$ units are sequentially bridged by bis(bidentate) oxalato ligands, resulting in an octahedral $O_4N_2$ donor set. Cryomagnetic susceptibility measurements show the occurrence of antiferromagnetic intrachain interactions for **2**, **3**, and **5**, whereas compound **1** exhibits a weak ferromagnetic coupling in agreement with the out-of-plane exchange pathway involved. The magnetic behavior of **1** and **2** is analyzed and discussed in the light of the available magneto-structural data for analogous systems. $Cd^{II}$ complex crystallizes in the monoclinic space group $C2/c$ with unit cell parameters of $a$ = 16.128(2) Å, $b$ = 6.757(1) Å, $c$ = 11.580(2) Å, $\beta$ = 104.46(1)°, and $Z$ = 4. Its crystal structure contains one-dimensional chains in which metal centers are heptacoodinated to four oxygen atoms from two symmetry-related bis(bidentate) oxalato bridges, two endocyclic nitrogen atoms of *trans*-coordinated triazole ligands and one water molecule, to give a $CdO_4O_wN_2$ pentagonal-bipyramidal geometry. Thermoanalytical and variable-temperature X-ray powder diffraction analyzes show that compound **6** undergoes a reversible dehydration–hydration process in which the anhydrous residue crystallizes with a different crystal lattice retaining the dimensionality of the oxalato–metal framework.


## Introduction

In recent years the area of inorganic crystal engineering[1] has become one of intense research activity due to the growing need for novel solid-state architectures with potential applications as functional materials in fields such as catalysis, conductivity, zeolitic behavior and magnetism.[2] The judicious choice of the metal ion, a well understanding of the coordination preferences of the bridging entities, and a careful selection of the terminal ligands are key steps for the rational design of metal-organic coordination polymers with novel topologies and specific chemical and physical properties.[3] In this context, the oxalato dianion, essentially as bridging ligand, has appeared as a very appealing tecton in constructing a great diversity of homo- and heterometallic compounds with interesting physical properties (magnetic, electric, or optical).[4] The prevalence of its rigid bis(chelating) bridging mode provides a degree of predictability with regard to the structural motifs, and architectures reported for oxalato coordination networks range from discrete oligonuclear species to high dimensionality (one-, two-, and three-dimensional) systems.[5] The formation of these structures largely depends on the shape of the templating counterions and/or the features of the auxiliary ligands used to complete the metal coordination sphere.

Without being exhaustive, 2D honeycomb-layered structures of general formula $[M^{II}M^{III}(ox)_3]^-$ ($M^{II}$ = V, Cr, Mn, Fe, Co, Ni, Cu, Zn; $M^{III}$ = V, Cr, Fe) are obtained with voluminous cations such as $[XR_4]^+$ (X = N, P; R = phenyl, *n*-propyl, *n*-butyl, *n*-pentyl), decamethylferrocenium, and tetrathiafulvalene derivatives.[6] The use of tris(chelated) transition-metal diimine complexes $[M(L)_3]^{m+}$ (L = 2,2-bipyridine or phenanthroline, $m$ = 2, 3) leads to helical 3D networks of formula $[M^{II}_2(ox)_3]^{2-}$, $[M^{II}M^{III}(ox)_3]^-$, and $[M^{I}M^{III}(ox)_3]^{2-}$ where cation and anion exhibit inverted chirality.[7] Discrete species are obtained by using polydentate N- and/or O-donor ligands that block most of the coordination sites around the metal center which precludes the formation of extended polymeric oxalato–metal systems of higher di-

[a] Departamento de Química Inorgánica, Facultad de Ciencia y Tecnología, Universidad del País Vasco,
Apartado 644, 48080 Bilbao, Spain
Fax: (internat) +34-94601-3500
E-mail: qipcacao@lg.ehu.es
qipluara@lg.ehu.es

Supporting information for this article is available on the WWW under http://www.eurjic.org or from the author.

mensionality.[8] Interestingly, in a series of previous papers, we have demonstrated that zigzag or linear one-dimensional complexes of formula $[M(\mu\text{-ox})(L)_x]_n$ ($M^{II}$ = Cu, Ni, Co) can be obtained by utilizing aromatic pyridyl moieties as monodentate terminal/axial ligands, which permits the polymerization process of the oxalato–metal framework.[9–11] This work aims (a) to develop standard synthesis routes (nature of reactants and synthetic conditions) to achieve a straight-forward design of one-dimensional oxalato–metal frameworks, (b) to study the influence of the structural features of these compounds on the magnetic interactions transmitted through the oxalato ligand, (c) to analyze the role of the terminal ligands in the type and magnitude of the crystalline interactions (essentially, hydrogen bonds and other non-covalent interactions between the aromatic systems of the pyridine rings), which ensure the cohesiveness of the crystal structure, and finally (d) to obtain analogous 1D systems with biological molecules such as nucleobases and other N-containing rings as terminal ligands. Indeed, our synthesis efforts have recently been successful with the isolation of a new family of 1D oxalato-bridged complexes in which the pyridinic bases are replaced by nucleobases such as purine and adenine, which behave as N-monodentate ligands.[12]

As a continuation of our research program concerning the use of structure-directing N-containing ligands in the synthesis of 1D oxalato network structures, herein we report the synthesis, crystal structures, and the magnetic behavior of a new family of complexes of formula $[M(\mu\text{-ox})(4atr)_2]_n$, where M = $Cu^{II}$, $Ni^{II}$, $Co^{II}$, $Fe^{II}$, $Zn^{II}$, and $[Cd(\mu\text{-ox})(4atr)_2(H_2O)]_n$ with the 4-amino-1,2,4-triazole ligand (4atr) acting as apical ligand with a quite unusual monodentate coordination mode. The use of the 1,2,4-triazole moiety as a part of ligand systems has gained considerable attention in recent years mainly because of the fact that it represents a hybrid of pyrazole and imidazole with regard to the arrangement of its heteroatoms, thus promising a rich and versatile coordination chemistry.[13]

## Results and Discussion

### $[M(\mu\text{-ox})(4atr)_2]$ [M = Cu (1), Ni (2), Co (3), Zn (4), Fe (5)]

Compounds **1**–**5** are isomorphous and crystallize in the triclinic space group $P\bar{1}$. Crystal parameters and details of the final refinements are summarized in Tables 1 and 2. Compounds **2**–**5** crystallize as poor-quality specimens, and therefore X-ray powder diffraction methods have been performed to obtain structural information (for Supporting Information see footnote on the first page of this article). The observed, calculated and difference X-ray powder diffraction patterns of compound **2** are shown in Figure 1. The

Table 1. Single-crystal data and structure refinement details of the compound $[Cu(\mu\text{-ox})(4atr)_2]_n$ (**1**).

| | | | |
|---|---|---|---|
| Empirical formula | $C_6H_8CuN_8O_4$ | $Z$ | 1 |
| Formula mass | 319.74 | $\rho_{calcd.}$ [g cm$^{-3}$] | 1.914 |
| Crystal system | triclinic | $\rho_{obsd.}$ [g cm$^{-3}$] | 1.91(1) |
| Space group | $P\bar{1}$ (no. 2) | $\mu$ [mm$^{-1}$] | 1.997 |
| $a$ [Å] | 5.538(1) | Reflections collected | 1689 |
| $b$ [Å] | 7.663(1) | Unique data/parameters | 1610/94 |
| $c$ [Å] | 7.711(2) | $R_{int}$ | 0.0283 |
| α [°] | 62.21(1) | Reflections with $I \geq 2\sigma(I)$ | 1451 |
| $\beta$ [°] | 73.91(1) | Goodness of fit ($S$) | 1.048 |
| $\gamma$ [°] | 86.11(1) | $R_1/wR_2$ [$I \geq 2\sigma(I)$] | 0.0685/0.1800 |
| $V$ [Å$^3$] | 277.4(1) | $R_1/wR_2$ [all data] | 0.0758/0.1841 |

$R_1 = \Sigma(|F_o| - |F_c|)/\Sigma|F_o|$. $wR_2 = [\Sigma w(F_o^2 - F_c^2)^2/\Sigma w(F_o^2)^2]^{1/2}$; $w = 1/[\sigma^2(F_o^2) + (0.1572P)^2]$ with $P = (|F_o|^2 + 2|F_c|^2)/3$.

Table 2. X-ray powder crystal data for compounds **2**–**4**.

| Compound | **2** | **3** | **4** |
|---|---|---|---|
| Empirical formula | $C_6H_8N_8NiO_4$ | $C_6H_8CoN_8O_4$ | $C_6H_8N_8O_4Zn$ |
| Formula mass | 314.87 | 315.11 | 321.57 |
| Crystal system | triclinic | triclinic | triclinic |
| Space group | $P\bar{1}$ (no. 2) | $P\bar{1}$ (no. 2) | $P\bar{1}$ (no. 2) |
| $a$ [Å] | 5.386(1) | 5.461(1) | 5.455(1) |
| $b$ [Å] | 7.716(1) | 7.741(1) | 7.769(1) |
| $c$ [Å] | 7.946(1) | 7.978(1) | 8.002(1) |
| α [°] | 60.87(1) | 60.96(1) | 60.93(1) |
| $\beta$ [°] | 76.54(1) | 76.33(1) | 76.34(1) |
| $\gamma$ [°] | 89.66(1) | 89.62(1) | 89.64(1) |
| $V$ [Å$^3$] | 278.3(1) | 284.2(1) | 285.7(1) |
| $Z$ | 1 | 1 | 1 |
| $\rho_{obsd.}$ [g cm$^{-3}$] | 1.87(1) | 1.84(1) | 1.86(1) |
| $\rho_{calcd.}$ [g cm$^{-3}$] | 1.878 | 1.841 | 1.868 |
| $R_f/R_b$ [%] | 9.95/8.70 | 9.13/9.25 | 5.47/9.87 |
| $R_p/R_{wp}$ [%] | 9.57/13.29 | 8.88/11.76 | 10.06/13.72 |
| $\chi^2$ | 2.37 | 5.50 | 6.30 |

$R_f = \Sigma|(I_{obsd.})^{1/2} - (I_{calcd.})^{1/2}|/\Sigma(I_{obsd.})^{1/2}$; $R_b = \Sigma|I_{obsd.} - I_{calcd.}|/\Sigma I_{obsd.}$; $R_p = \Sigma|yi_{obsd.} - yi_{calcd.}|/\Sigma yi_{obsd.}$; $R_{wp} = [\Sigma wi|yi_{obsd.} - yi_{calcd.}|^2/\Sigma wi(yi_{obsd.})^2]^{1/2}$.

  

XRPD pattern of **5** shows preferred orientation effects and it has only allowed a structureless pattern matching analysis giving a centric triclinic unit cell with $a$ = 5.685(1) Å, $b$ = 7.773(1) Å, $c$ = 8.110(1) Å, $\alpha$ = 61.27(2)°, $\beta$ = 72.16(2)°, $\gamma$ = 87.29(1)°, and $V$ = 297.0(1) Å$^3$.

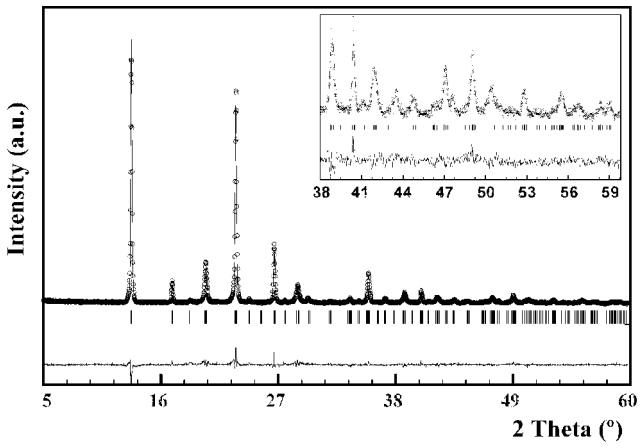


Figure 1. Final Rietveld plot for compound **2**. The observed data are shown by the dots, the calculated pattern by the solid line, and the lower trace corresponds to the difference between observed and calculated patterns.

The crystal structures of **1**–**4** are built up of *trans*-$[M(4atr)_2]^{2+}$ units joined sequentially by centrosymmetric bis(bidentate) oxalato ligands to form polymeric linear chains running parallel to the *a*-axis. The separation of the $M^{II}$ atoms along the chains varies from 5.386(1) Å (**2**) to 5.538(1) Å (**1**). The metal atoms, located on crystallographic inversion centers, are coordinated to four oxygen atoms of two bridging oxalato ligands, and two endocyclic nitrogen atoms from two crystallograhically related 4atr molecules, resulting in octahedral $MO_4N_2$ donor sets. A perspective view of the polymeric chain of **1** is given in Figure 2, whereas selected bond lengths and angles are gathered in Table 3.

Table 3. Selected bond lengths [Å] and angles [°] for $[M(\mu\text{-ox})(4atr)_2]_n$ [M = Cu (**1**), Ni (**2**), Co (**3**) and Zn (**4**)].

| | Cu (**1**) | Ni (**2**) | Co (**3**) | Zn (**4**) |
|---|---|---|---|---|
| M–O1 × 2 | 1.986(3) | 2.10(1) | 2.15(1) | 2.14(1) |
| M–O2 × 2 | 2.307(3) | 2.06(1) | 2.07(1) | 2.07(1) |
| M–N11 × 2 | 2.003(3) | 2.16(1) | 2.26(1) | 2.31(1) |
| O1–M–O2 | 77.5(1) | 80.8(1) | 79.5(1) | 79.6(1) |
| O1–M–N11 | 89.8(1) | 93.8(1) | 86.4(1) | 89.5(1) |
| O1–M–N11a | 90.2(1) | 86.2(1) | 93.6(1) | 90.5(1) |
| O1–M–O1a | 180(–) | 180(–) | 180(–) | 180(–) |
| O1–M–O2a | 102.5(1) | 99.2(1) | 100.5(1) | 100.4(1) |
| O2–M–N11 | 90.3(1) | 85.3(1) | 89.9(1) | 87.3(1) |
| O2–M–N11a | 89.7(1) | 94.7(1) | 90.1(1) | 92.7(1) |
| O2–M–O2a | 180(–) | 180(–) | 180(–) | 180(–) |
| N11–M–N11a | 180(–) | 180(–) | 180(–) | 180(–) |

Symmetry code: (a) $-x$, $-y$, $2-z$

The most striking difference between the polymeric chains is the expected tetragonal Jahn–Teller elongation of the copper(II) octahedron in **1**, with two *trans* axial bond lengths [Cu–O2: 2.307(3) Å] substantially longer than the equatorial ones (ca. 2.00 Å). The difference of the Cu–O bond lengths (0.31 Å) involving the bis(bidentate) oxalato ligand is similar to those observed in other six-coordinate copper(II) complexes based on asymmetrically coordinated oxalato bridges.[14–16] The atoms involved in the four short bonds (O1, O1a, N11, N11a) define the equatorial plane of the $MO_4N_2$ chromophore that forms a dihedral angle of 83.5° with the oxalato bridging ligand.

Compounds **2**, **3** and **4** exhibit a rather typical octahedral metal(II) coordination with $M–O_{ox}$ bond lengths similar to those found in other oxalato-bridged metal(II) complexes (Ni: 1.960–2.152 Å; Co: 2.051–2.212 Å; Zn: 2.011–2.271 Å) registered in the Cambridge Structural Database (CSD, March 2005 release).[17] The triazole ligand is coordinated to the metal atom through the endocyclic N11 atom of the pentagonal ring[18] and it is perpendicular to the oxalato–metal framework (ca. 89°). The rings are arranged along the growing axis of the polymeric chain owing to an intra-

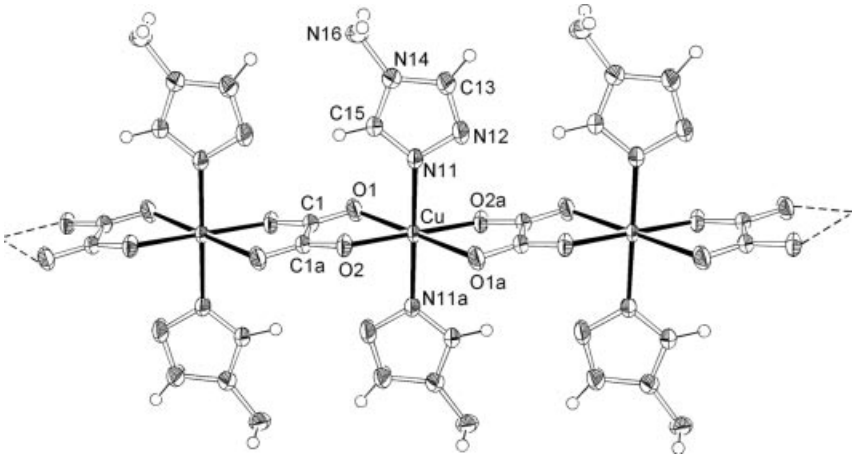


Figure 2. Perspective drawing of the polymeric chain of **1**. Thermal ellipsoids are drawn at the 50% probability level. Symmetry code: (a) $-x$, $-y$, $2-z$.

  

molecular C–H···N hydrogen bond that is established between two consecutive 4atr ligands of the same side of the chain [C15···N12: 3.381(5) Å, C15–H15···N12: 166° for compound **1**]. The hydrogen atoms of the exocyclic amino group of the apical ligands are projected forward to the outside of the chains which allows their involvement in an extended network of N–H···$O_{ox}$ hydrogen bonds with the oxalato oxygen atoms belonging to adjacent chains which sustains the supramolecular 3D structure of the complexes (Figure 3). The hydrogen-bonded chains are related by crystallographic inversion centers with a chain···chain distance coincident with the *c* parameter of the unit cell [from 7.711(2) Å for **1** to 8.002(1) Å for **4**]. Crystal building of these compounds can be alternatively described as a pillar-layered structure based on sheets of neutral oxalato–metal chains along the *ab* plane and triazole ligands perpendicularly inserted in the interlamellar region. Each organic molecule serves as pillar to link adjacent inorganic sheets. It is directly bound to a metal center of a sheet and its hydrogen-bonding donor is attached to the adjacent one supporting the cohesiveness of the layered structure.

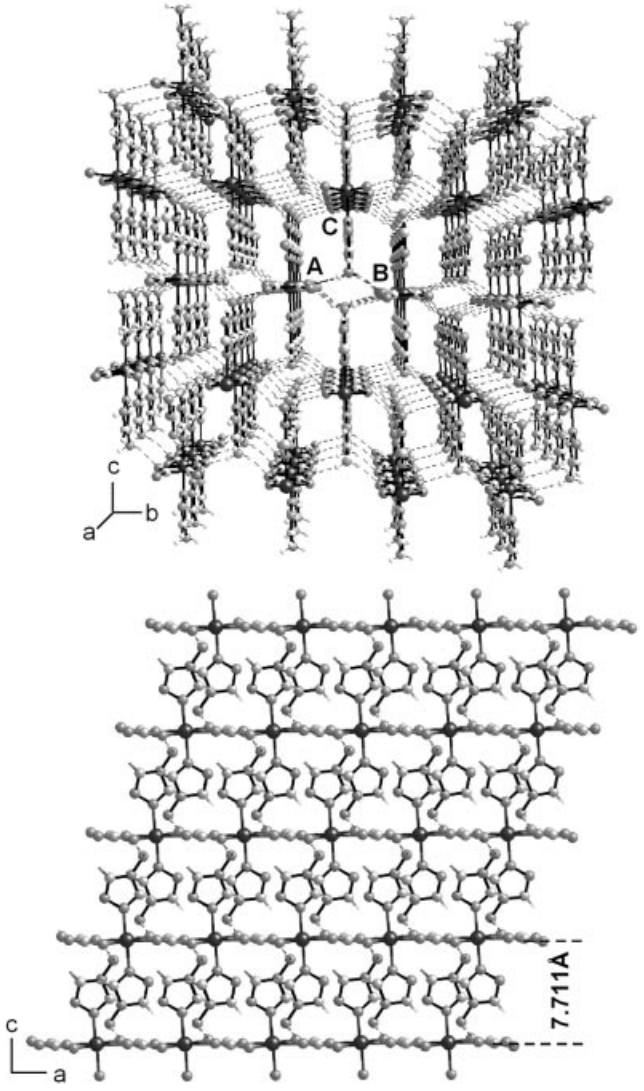


Figure 3. Views of the crystal packing of compound **1** showing the hydrogen bonds (dashed lines) and the layered structure. Intrachain distances [Å]: A···B = 7.663(1) (*b* parameter of the unit cell); A···C = 7.711(2) (*c* parameter).

The thermal degradation of compounds **1**–**5**, deduced from their TG and DTA curves in synthetic air (see Supporting Information), clearly indicates that the overall supramolecular three-dimensional architecture of all compounds is quite stable. The metal-organic framework of **1** retains its rigidity and stability up to 200 °C after which three exothermic processes take place to give copper(II) oxide as a final black powdery product above 500 °C. The three-dimensional cohesiveness of the remaining crystal structures is more robust and they undergo a first exothermic degradation process with an on-set temperature of approximately 325 °C for **2**, 310 °C for **3**, 250 °C for **4**, and 255 °C for **5**. In all the cases, the thermal degradation is completed above 500 °C to yield the metal(II) oxide (**2** and **4**) or $M_2O_3$ (**3** and **5**) as final products.

The temperature dependence of the $\chi_M T$ product ($\chi_M$ is the magnetic susceptibility per copper atom) and the variation of the inverse susceptibility ($\chi_M^{-1}$) for compound **1** are shown in Figure 4. The $\chi_M T$ values increase continuously, upon cooling, from 0.418 $cm^3$ $mol^{-1}$ K at room temperature up to a value of 0.920 $cm^3$ $mol^{-1}$ K at 2.0 K. Above 15 K, thermal variation of $\chi_M^{-1}$ is well described by the Curie–Weiss law with a $\theta$ value of +4.12 K. That is indicative of the predominance of ferromagnetic interactions between the metal centers. The magnetic data were successfully fitted by a numerical expression proposed for uniform copper(II) chains with ferromagnetic[19] intrachain interactions derived through the Hamiltonian $H = -J\Sigma S_i S_{i+1}$. The best-fitted values were $J = +2.18\ cm^{-1}$, $g = 2.16$ and $R = 2.0 \times 10^{-5}$. The agreement factor $R$ is defined as $\Sigma_i[(\chi_M T)_{obsd.}(i) - (\chi_M T)_{calcd.}(i)]^2/\Sigma_i[(\chi_M T)_{obsd.}(i)]^2$.

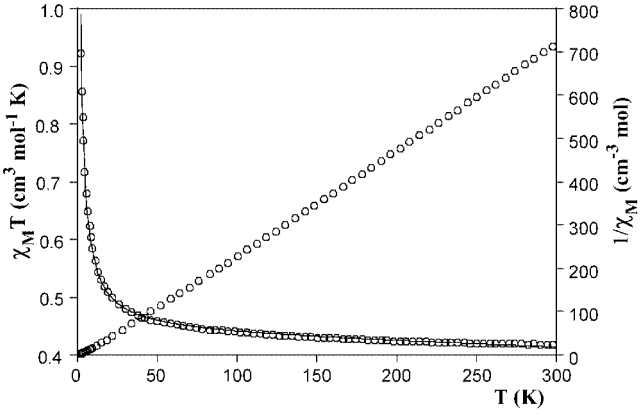


Figure 4. Thermal dependence plots of $\chi_M T$ and $1/\chi_M$ for compound **1**. (−) best theoretical fit (see text).

For oxalato-bridged $Cu^{II}$ complexes it has been found[9–12,20] that the value and type of the magnetic coupling is essentially governed by the magnitude of the overlap between the symmetry-adapted highest occupied molecular orbitals (HOMOs, $\sigma$ symmetry) of the oxalato ligand and the metal-centered magnetic orbitals (mainly, a $d_{x^2-y^2}$-type

  

orbital in square-pyramidal or tetragonally elongated octahedral geometries) which are defined by the short equatorial (or basal) copper–ligand bonds. The strongest antiferromagnetic coupling (values of $J$ ranging from –260 to –400 $cm^{-1}$)[12,20,21] result when the oxalato bridge is symmetrically coordinated with two short bonds to each copper(II) center in such a way that it is coplanar with the singly occupied molecular orbitals (SOMOs) of the copper atoms. But when one copper–bridge distance is long (i.e., oxalato bridge is asymmetrically coordinated), the two metal-centered magnetic orbitals are parallel to each other and perpendicular to the bridging ligand (Scheme 1), the interaction between the d magnetic orbitals through the oxalato ligand is poor, and a weak anti- or ferromagnetic (when the overlap is zero, accidental orthogonality)[9–11,14,20,22–25] coupling results, as occurs in **1**.

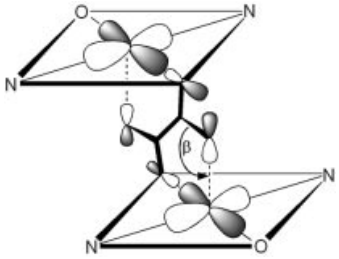


Scheme 1.

The magnetostructural data which are listed in Table 4 correspond to copper(II) complexes with an out-of-plane exchange pathway (perpendicular orbital arrangement). It shows that the value of the bond angle C–O–Cu involving the apical oxalate oxygen atom (β) is the main structural factor governing the nature of the magnetic interaction for the perpendicular topology between the oxalato and the copper(II) magnetic plane represented in Scheme 1. Compounds with $\beta \leq 109.5°$ show ferromagnetic interactions, whereas for $\beta > 109.5°$ the magnetic coupling between copper(II) ions is antiferromagnetic. This angle seems to be related to the overlap between the two metal-centered SOMOs and as a consequence to the sign of the magnetic exchange for the perpendicular topology. This magnetostructural result could be used to anticipate the magnetic interaction for new structurally characterized compounds based on oxalato-bridged copper(II) frameworks. For example, the two-dimensional $[Cu_3(\mu\text{-ox})_3(\mu\text{-bpy})_2(bpy)]_n$ polymer consists of sheets in which oxalato–copper(II) chains are crosslinked by bridging bidentate 4,4′-bypyridine ligands. The magnetic measurements show the occurrence of weak ferromagnetic interactions ($J = +0.6\ cm^{-1}$) transmitted through two asymmetrically coordinated oxalato bridges with $\beta < 108.3°$.[26]

Figure 5 shows the magnetic behavior of compounds **2**, **3** and **5**. The thermal dependence of the molar magnetic susceptibility, $\chi_M$, of compound **2** shows a maximum at 44 K which is characteristic of antiferromagnetic interactions between the nickel(II) centers. The magnetic data of compound **2** were fitted by numerical expressions proposed for $S = 1$ chains with uniform antiferromagnetic interactions.[27] The results of the best fits were $J = -23.7\ cm^{-1}$, $g = 2.10$, $\rho = 0.010$ and $R = 4.0 \times 10^{-5}$. The percentage of paramagnetic impurities per mol of nickel atom is $\rho$ (assuming that the molecular weight of the impurity is the same as that of the investigated compound). Previous magnetostructural studies of dinuclear oxalato-bridged $Ni^{II}$ complexes have revealed that the magnitude of the exchange coupling constant is strongly dependent on the nature of the donor atoms in the peripheral ligands: the less electronegative they are, the greater the antiferromagnetic coupling is. This effect is more marked when the less electronegative donor atoms are coplanar with the bridging oxalato ligand.[9,28] The observed $J$ value for compound **2** ($-23.7\ cm^{-1}$) compares well with that reported for the

Table 4. Selected magnetostructural data ([Å], [°], [$cm^{-1}$]) for oxalato-bridged copper(II) complexes having out-of-plane exchange pathway.

| Compound[a] | Cu–$O_{ax}$ | Cu···Cu | $h$(Cu) | $\gamma$ | $\beta$ | $J$ | Ref. |
|---|---|---|---|---|---|---|---|
| $[Cu_2(\mu\text{-ox})(bpcam)_2(H_2O)_2]$ | 2.44 | 5.68 | 0.00 | 101.8 | 106.6 | +0.8 | [23] |
| $[Cu_2(\mu\text{-ox})(bpca)_2(H_2O)_2]$ | 2.41 | 5.63 | 0.05 | 80.7 | 106.9 | +1.0 | [25] |
| $[Cu(\mu\text{-ox})(2apy)_2]_n$ | 2.38 | 5.63 | 0.02 | 75.6 | 107.8 | +2.0 | [9] |
| $[Cu(\mu\text{-ox})(4atr)_2]_n$ | 2.31 | 5.54 | 0.00 | 83.5 | 108.0 | +2.2 | this work |
| $[Cu(\mu\text{-ox})(py)_2]_n$ | 2.27 | 5.46 | 0.00 | 80.8 | 108.0 | +1.4 | [15] |
| $\{[Cu(\mu\text{-ox})(bpy)]\cdot 2H_2O\}_n$[b] | 2.31 | 5.55 | 0.03 | 83.4 | 108.5 | +2.4 | [14] |
| | 2.32 | 5.56 | | 83.4 | 108.3 | | |
| $\{[Cu(\mu\text{-ox})(tmen)]\cdot 4H_2O\}_n$[b] | 2.35 | 5.60 | 0.01 | 81.2 | 108.3 | +0.3 | [16] |
| | 2.38 | 5.66 | | 78.4 | 108.7 | | |
| $[Cr_2Cu_2(\mu\text{-ox})_5(bpy)_4]\cdot 2H_2O$ | 2.25 | 5.44 | 0.03 | 81.7 | 108.8 | +2.0 | [24] |
| $[Cu(\mu\text{-ox})(pyOH)_2]_n$ | 2.28 | 5.55 | 0.00 | 81.9 | 109.2 | +1.3 | [10] |
| $[Cu(\mu\text{-ox})(isq)_2]_n$ | 2.23 | 5.48 | 0.06 | 88.5 | 109.5 | +0.6 | [11] |
| $[Cu(\mu\text{-ox})(4apy)_2]_n$ | 2.35 | 5.66 | 0.00 | 88.7 | 109.7 | –1.1 | [9] |
| $\{[Cu(\mu\text{-ox})(3apy)_2]\cdot 1.5H_2O\}_n$ | 2.21 | 5.46 | 0.00 | 85.2 | 111.0 | –1.3 | [9] |
| $[Cu_2(\mu\text{-ox})(bpmen)_2](ClO_4)_2$ | 2.18 | 5.49 | 0.00 | 88.2 | 111.6 | –2.1 | [8a] |

[a] Abbreviations used: Cu–$O_{ax}$: copper–oxalate oxygen axial bond. Cu···Cu: copper–copper separation across the bridging oxalato ligand. $h$(Cu): Displacement of the copper atom out of the basal plane. $\gamma$: dihedral angle between the equatorial and oxalato mean planes. $\beta$: C–O–Cu angle involving the apical oxalato oxygen atom. bpy = 2,2-bipyridine; 2apy = 2-aminopyridine; py = pyridine; pyOH = 3-hydroxypyridine; isq = isoquinoline; tmen = *N*,*N*,*N*′,*N*′-tetramethylethylenediamine; 4apy = 4-aminopyridine; 3apy = 3-aminopyridine; bpmen = *N*,*N*′-bis(2-pyridylmethyl)-*N*,*N*′-dimethyl-1,2-ethanediamine; bpca = bis(2-pyridylcarbonyl)amidate; bpcam = bis(2-pyrimidylcarbonyl)-amidate. [b] The compound presents two crystallographically independent oxalato bridges.

  

1D-[Ni(μ–ox)(4apy)$_2$]$_n$ (4apy = 4-aminopyridine) ($J$ = –24.4 cm$^{-1}$)[9] that also shows a *trans*-$NiO_4N_2$ chromophore, but it is somewhat lower than those reported for other one-dimensional complexes with a *cis*-$NiO_4N_2$ environment ($J$ varies between –26.8 and –31.3 cm$^{-1}$).[9,11]

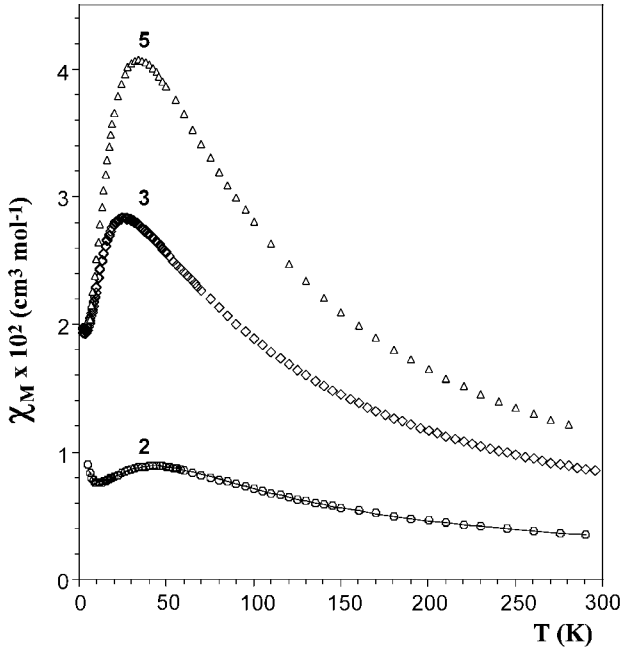


Figure 5. Thermal dependence plots of $\chi_M$ for the nickel(II) (**2**), cobalt(II) (**3**), and iron(II) (**5**) compounds; (–) best theoretical fit for **2** (see text).

The molar magnetic susceptibility ($\chi_M$) values of compounds **3** and **5** increase when the temperature decreases, reaching a maximum at approximately 26 (**3**) and 35 K (**5**), with values of $2.83 \times 10^{-2}$ for **3** and $4.07 \times 10^{-2}$ cm$^3$ mol$^{-1}$ for **5**, and then decreases very quickly. The $\chi_M T$ curves exhibit a continuous decrease upon cooling. This behavior suggests the presence of a moderate antiferromagnetic coupling between the magnetic centers through the bridging oxalato ligand. The experimental effective magnetic moments at room temperature of 5.00 (**3**) and 5.64 $\mu_B$ (**5**) are larger than the spin-only values of 3.87 $\mu_B$ for an uncoupled high-spin cobalt(II) ion ($S$ = 3/2) and 4.90 $\mu_B$ for a high spin $Fe^{II}$ center ($S$ = 2). This behavior is typical of cobalt(II) and iron(II) ions in distorted octahedral geometries and a large orbital contribution to the magnetic moment should be considered.[9,11,24,29]

The quantitative analysis of the magnetic properties for systems involving ions with a significant orbital contribution is a difficult task. All our attempts to reproduce the experimental data of the compounds **3** and **5** by using the classical spin Heissenberg chain model[30] with $S$ = 3/2 (Co) and $S$ = 2 (Fe) or by fitting the low-temperature data (for **3**) as collections of Ising chains $S$ = 1/2 effective spins with antiferromagnetic interactions were unsuccessful.[9,31,32] However, it is necessary to note that the magnetism curves and the $\chi_{max}$ and $T_{max}$ values for complexes **3** and **5** are similar to those reported for polynuclear oxalato-bridged metal(II) complexes containing these paramagnetic centers with $J$ values up to –25 cm$^{-1}$ (Co)[8a,32] and –10 cm$^{-1}$ (Fe).[32a,33] There are no known examples where the oxalate ion mediates a ferromagnetic interaction.

### [Cd(μ-ox)(4atr)$_2$(H$_2$O)]$_n$ (6)

Crystal parameters and refinement results for compound **6** are summarized in Table 5. Its crystal structure consists of zigzag polymeric chains in which the $Cd^{II}$ centers are sequentially bridged by bis(bidentate) oxalato ligands. The intrachain Cd···Cd distance across the oxalato bridge is 6.068(1) Å with a Cd···Cd···Cd angle between three consecutive atoms of 145(1)°. A detailed picture of a one-dimensional fragment is shown in Figure 6. Values of selected bond lengths and angles are reported in Table 6. The distorted pentagonal-bipyramidal coordination about each $Cd^{II}$ center is completed by a water molecule [Cd–O3w: 2.431(9) Å] in the equatorial plane and the N11 endocyclic nitrogen atoms of two triazole ligands [2.321(6) Å] in the apical positions with an N11–Cd–N11a angle of 168.4(4)°, to give a $CdO_4O_wN_2$ donor set with a twofold axis along the Cd–O3w bond. The centrosymmetric oxalato bridge is coordinated with two similar Cd–O distances [Cd–O1: 2.331(6) Å, Cd–O2: 2.422(6) Å]. These values are typical of $Cd^{II}$ complexes based on bis(bidentate) oxalato ligands.[34] The bite angle O1–Cd–O2 [70.1(2)°] is similar to those reported for oxalato-bridged cadmium(II) complexes with a pentagonal-bipyramidal coordination (range from 66 to 71°), but it is lower than the octahedral ones (72–74°).[17] The two symmetry-related oxalato ligands around the metal

Table 5. Single-crystal data and final refinement details of the compound [Cd(μ-ox)(4atr)$_2$(H$_2$O)]$_n$ (**6**).

| | | | |
|---|---|---|---|
| Empirical formula | $C_6H_{10}CdN_8O_5$ | Z | 4 |
| Formula mass | 386.62 | $\rho_{calcd.}$ [g cm$^{-3}$] | 2.102 |
| Crystal system | monoclinic | $\rho_{obsd.}$ [g cm$^{-3}$] | 2.09(1) |
| Space group | *C*2/*c* (no. 15) | $\mu$ [mm$^{-1}$] | 1.825 |
| *a* [Å] | 16.128(2) | Reflections collected | 4581 |
| *b* [Å] | 6.757(1) | Unique data/parameters | 1185/101 |
| *c* [Å] | 11.580(2) | $R_{int}$ | 0.0730 |
| α [°] | 90 | Reflections with $I \geq 2\sigma(I)$ | 787 |
| *β* [°] | 104.46(1) | Goodness of fit [*S*] | 1.068 |
| *γ* [°] | 90 | $R_1/wR_2$ [$I \geq 2\sigma(I)$] | 0.0428/0.0882 |
| *V* [Å$^3$] | 1222.0(3) | $R_1/wR_2$ [all data] | 0.0815/0.0988 |

$R_1 = \Sigma(|F_o| - |F_c|)/\Sigma|F_o|$; $wR_2 = [\Sigma w(F_o^2 - F_c^2)^2/\Sigma w(F_o^2)^2]^{1/2}$; $w = 1/[\sigma^2(F_o^2) + (0.0442P)^2]$ with $P = (|F_o|^2 + 2|F_c|^2)/3$.

  

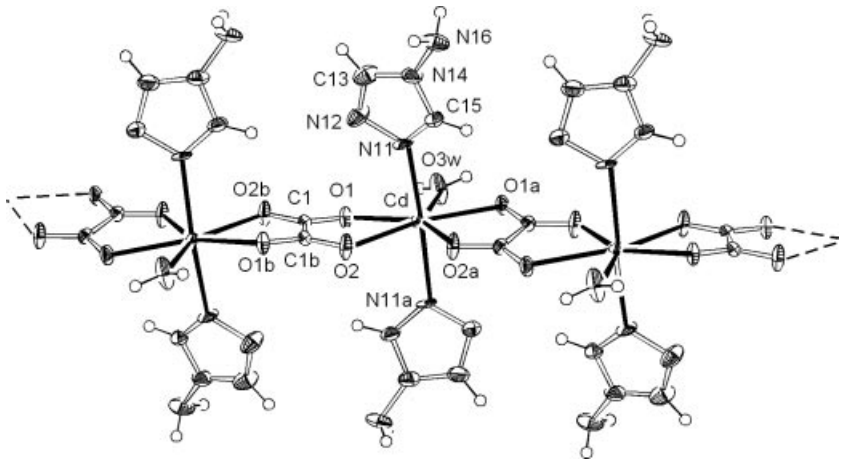


Figure 6. ORTEP drawing of a fragment of the polymeric chain of compound **6**. Symmetry code: (a) 1 – *x*, *y*, 3/2 + *z*; (b) 1 – *x*, –*y*, 2 – *z*.

atom are essentially planar and they are twisted to each other by 11.5(3)°. The cadmium atoms are displaced 0.39(1) Å out of the oxalate plane. The *trans*-coordinated triazole ligands are nearly parallel to the propagation direction of the chain (7.8°) and they are tilted with respect to each other and to the metal equatorial mean plane by 26.9 and 80.5°, respectively.

Table 6. Selected bond lengths [Å] and angles [°] for compound **6**.

| | | | |
|---|---|---|---|
| Cd–O1 × 2 | 2.331(6) | Cd–O2 × 2 | 2.422(6) |
| Cd–O3w | 2.431(9) | Cd–N11 × 2 | 2.321(6) |
| O1–Cd–O2 | 70.1(2) | O2–Cd–O3w | 142.6(1) |
| O1–Cd–O3w | 72.6(2) | O2–Cd–N11 | 84.2(2) |
| O1–Cd–N11 | 93.7(2) | O2–Cd–O2a | 74.8(3) |
| O1–Cd–O1a | 145.3(3) | O2–Cd–N11a | 86.7(2) |
| O1–Cd–O2a | 144.6(2) | O3w–Cd–N11 | 95.8(2) |
| O1–Cd–N11a | 89.8(2) | N11–Cd–N11a | 168.4(4) |

Symmetry code: (a) 1 – *x*, *y*, 3/2 – *z*

The polymeric chains grow along the *c*-axis of the unit cell, and each coordinated water molecule forms two hydrogen bonds, related by a twofold axis, with the O2 oxygen atom from two consecutive oxalato bridges belonging to a neighboring chain with an interchain Cd···Cd distance of 6.757(1) Å (*b* parameter). These $O_w$–$H_w$···$O_{ox}$ interactions give rise to sheets, which are spreading out along the crystallographic *bc* plane (Figure 7). The triazole rings are pointing in a direction almost perpendicular to the layers (in the inter-lamellar region) and crosslink adjacent sheets by means of the N–H···$O_{ox}$ hydrogen bonds involving the exocyclic amino group and the oxalato oxygen atoms belonging to two adjacent chains with Cd···Cd and chain···chain distances of 8.813 and 8.064 Å, respectively.

The analysis of the crystal packing clearly shows that the coordinated water molecules are located in unobstructed microchannels along the *c*-axis. This arrangement is able to facilitate the reversible transport of the water molecules along the channels and allows an understanding of why the dehydration temperature of the compound **6** falls within the lower range of values reported for the loss of coordinated water molecules.[35] Thermogravimetric curves (TG/DTA) of compound **6** are portraited in Figure 8. The release of

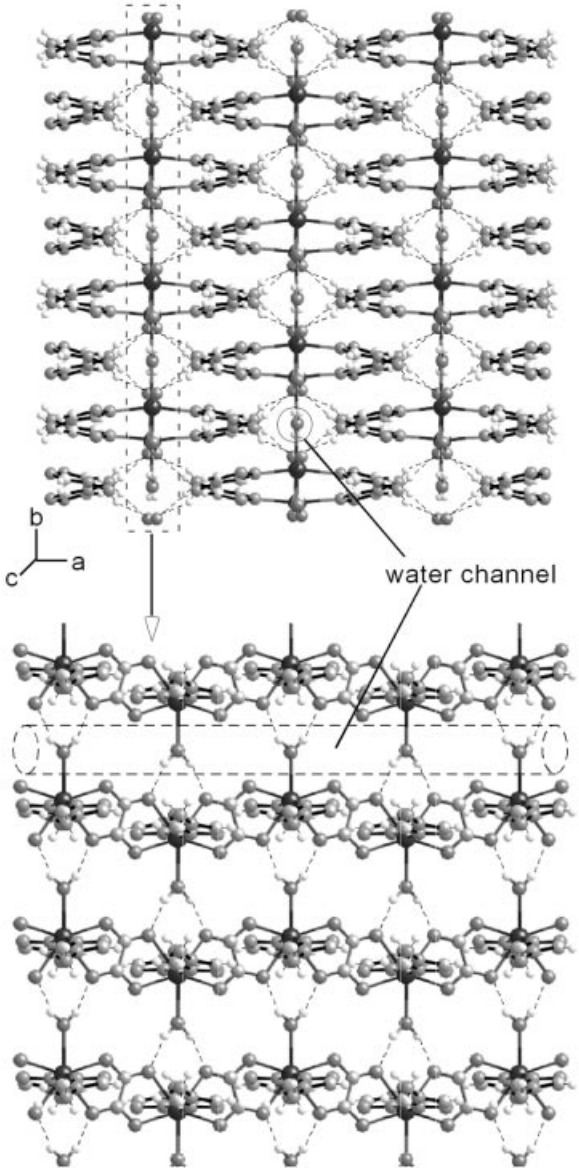


Figure 7. Crystal packing of compound **6** (hydrogen bonds are indicated by dashed lines).

  

the water molecule is an endothermic process that starts at 90 °C and is completed by about 110 °C (DTA peak: 100 °C; weight loss: exp. 4.70%, calcd. 4.66%). The anhydrous compound **7** is stable up to 290 °C and then it undergoes three successive exothermic processes (DTA peaks: 310, 380 and 515 °C) leading to CdO above 520 °C, with a total weight loss of 67.60% (calcd. 66.79%).

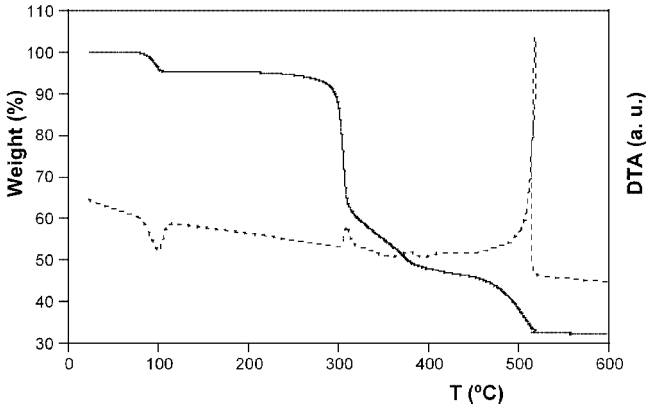


Figure 8. Thermogavimetric curves (TG/DTA) of compound **6** from room temperature to 600 °C.

Although crystal shape and size seem to be initially retained during the loss of the coordinating water molecule, single crystals of **6** lose gradually luster and become effectively a polycrystalline powder, precluding the in-situ structure determination from single-crystal diffraction techniques. Nevertheless, variable-temperature X-ray powder diffraction measurements (XRPD) revealed that the sample remains crystalline (Figure 9). The XRPD profile at 135 °C of **7** is not only substantially different than that obtained for the original compound, but also shows marked differences with the ones of the above-described compounds **1**–**5** (Figure 10). In a first approach, the powder pattern of **7** has been indexed in the orthorhombic space group *Pnmn* with unit cell parameters of $a$ = 5.915(2) Å, $b$ = 7.408(4) Å, $c$ = 14.210(2) Å. These values are comparable to those found for the one-dimensional $[Mn(\mu\text{-ox})(4atr)_2]_n$ compound[36] except for a significant elongation of the crystallographic parameter $a$.

The $Mn^{II}$ complex contains linear one-dimensional chains similar to those described for the triclinic compounds **1**–**4** where the M···M distance across the oxalato bridge also coincides with the repeat distance of the $a$-axis [5.599(1) Å for Mn]. The subtle difference between the $Mn^{II}$ crystal structure and those of the above described compounds is the greater parallel displacement of the neighboring chains of the $Mn^{II}$ compound. The hydrogen-bonded polymeric chains are related through a symmetry center in compounds **1**–**5**, whereas they are related through twofold axes in the $Mn^{II}$ complex in such a way that the observed value of 5.915(2) Å for the fully anhydrous compound might be the Cd···Cd intrachain distance, and it is within the range found for other oxalato-bridged $Cd^{II}$ complexes (5.827–6.213 Å).[17] Therefore, the Mn complex and the dehydrated $Cd^{II}$ compound seem to be isostructural and it is

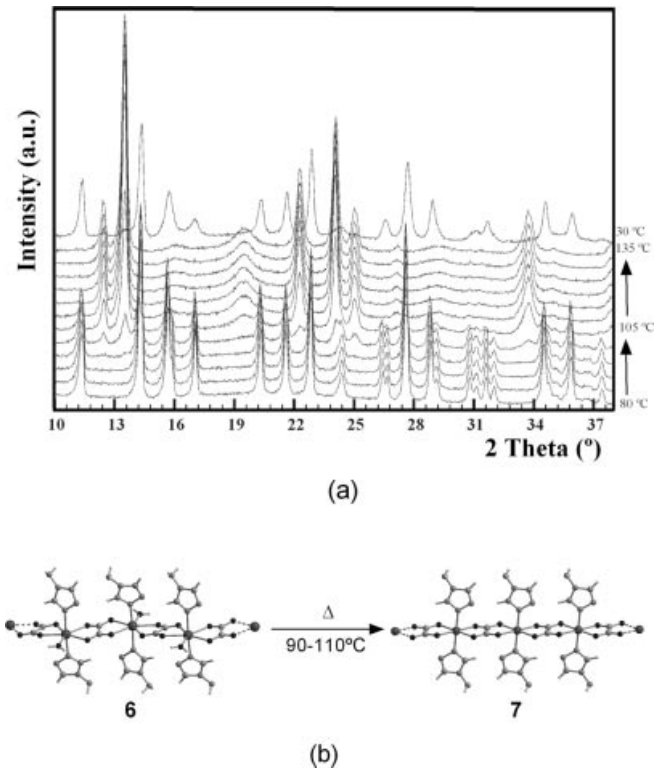


Figure 9. (a) Variable-temperature XRPD patterns of compound **6**. The last one was performed at room temperature 12 h after cooling. (b) Drawing of the polymeric chains of compounds **6** and the tentative structure of the anhydrous one (**7**) above 110 °C.

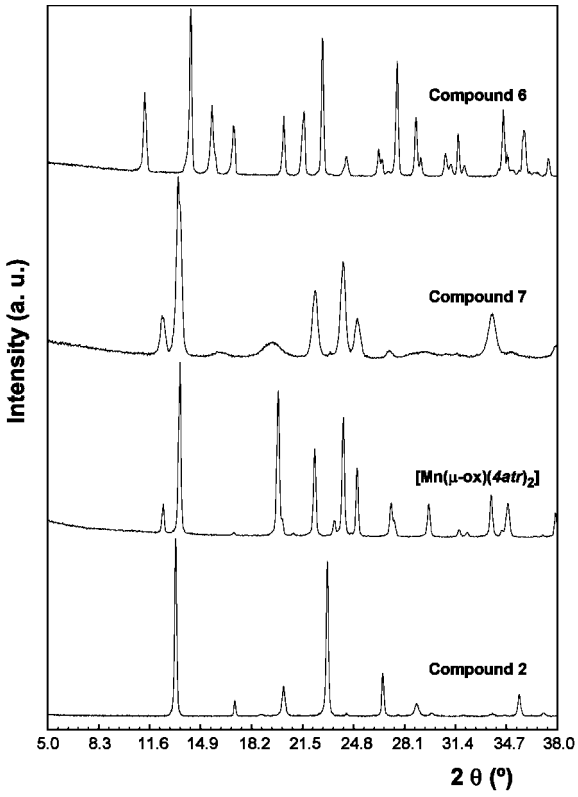


Figure 10. Diffraction patterns for compounds **2**, **6**, **7** and the analogous $[Mn(\mu\text{-ox})(4atr)_2]_n$.

  

likely that the loss of the coordinated water molecule provides an octahedral coordination environment around the $Cd^{II}$ atoms with a slight distortion of the oxalato–metal framework, but the initial overall 1D structure of the polymeric chain is retained without a drastic structural rearrangement (Figure 9b). In addition, thermogravimetric and X-ray powder crystallographic analyses indicate that the dehydration process is reversible. Upon exposure of **7** to air at room temperature for 12 h, it changed back to the initial aqua form, and the crystallinity was again retained. The system does not suffer any noticeable fatigue after repeating several **6** ↔ **7** cycles. It deserves to note that the references in the literature concerning the reversible loss of coordinated water molecules with no loss of crystallinity are scarce.[37] Usually, the residue is poorly crystalline (even amorphous) or its anhydrous crystal lattice shows a substantial rearrangement of the structural units that precludes the reversibility of the process.

## Conclusions

Complexes **1**–**6** are examples of crystal engeneering, because we show how the 4-amino-1,2,4-triazole can be used as terminal ligand towards oxalato–metal frameworks to afford one-dimensional architectures, as previously thought. The analysis of structural and magnetic data of compound **1** and another related oxalato-bridged copper(II) complexes with an out-of-plane exchange pathway clearly evidences the influence of the C–O–Cu angle on the type of the magnetic coupling. This trend would provide a useful tool to predict the behavior of new magnetic compounds. The Cd complex is one of the few examples that shows a reversible release of coordination water molecules, the anhydrous compound remains crystalline but with a different phase.

## Experimental Section

**Reagents:** All chemicals were of reagent grade and were used as commercially obtained. Standard literature procedures were used to prepare the starting materials Co(ox)·$2H_2O$, Ni(ox)·$2H_2O$, $K_2$[Cu(ox)$_2$]·$2H_2O$ and Cd(ox)·$3H_2O$.[38]

**Physical Measurements:** Elemental analyses (C, H, N) were performed with a Perkin–Elmer 2400 microanalytical analyser. Metal content was determined by absorption spectrometry. The purity and homogeneity of the polycrystalline samples of **1**–**6** used for physical measurements were checked by IR spectroscopy, elemental analysis, and X-ray powder diffraction methods.[39] The IR spectra (KBr pellets) were recorded with a Nicolet 740 FT-IR spectrometer in the 4000–400 $cm^{-1}$ spectral region. Magnetic measurements were performed on polycrystalline samples of the complexes taken from the same uniform batches used for the structural determinations with a Quantum Design SQUID susceptometer covering the temperature range 2.0–300 K at a magnetic field of 1000 G. The susceptibility data were corrected for the diamagnetism estimated from Pascal's tables,[40] the temperature-independent paramagnetism and the magnetization of the sample holder. Thermal analyses (TG/DTA) were performed with a TA Instruments SDT 2960 thermal analyser in synthetic air (79% $N_2$/21% $O_2$) with a heating rate of 5 °C $min^{-1}$. A prismatic blue crystal of **1** (0.15 × 0.06 × 0.06 mm) and a prismatic colorless crystal of **6** (0.10 × 0.10 × 0.06 mm) were selected for the structural analysis. Diffraction data were collected at 293(2) K with Enraf–Nonius CAD4 automatic four-circle (**1**) and Oxford Diffraction Xcalibur (**6**) diffractometers with graphite-monochromated Mo-$K_\alpha$ radiation ($\lambda$ = 0.71069 Å). Unit-cell parameters and orientation matrix of **1** were determined by least-squares treatment of the setting angles of 25 reflections on the range $4° < \theta < 13°$. Indexation and unit-cell refinement of **6** were based on all observed reflections from 10 frames collected with an oscillation range of 1°/frame and an exposure time of 3 min/frame. The data reduction was done with the XCAD[41] and CrysAlis RED[42] programs for compounds **1** and **6**, respectively. Both structures were solved by direct methods using the SIR92 program[43] and refined by full-matrix least squares on $F^2$ including all reflections (SHELXL93).[44] All calculations were performed using the WINGX crystallographic software package.[45] The final geometrical calculations and the graphical manipulations were carried out with the PARST95[46] and PLATON[47] programs. The X-ray powder diffraction (XRPD) patterns of compounds **2**–**5** were collected with a Phillips X'PERT powder diffractometer with Cu-$K_\alpha$ radiation over the range $5° < 2\theta < 60°$ with a fixed-time counting of 6–25 s at 25 °C. Indexation of the diffraction profiles of compounds **2**–**5** was made by means of the FULLPROF program (pattern-matching analysis)[48] on the basis of the space group and the cell parameters found for compound **1**. The atomic coordinates of **1** have been used as starting values for a least-squares refinement based on fitting the calculated and observed intensity profiles of an XRPD pattern of compounds **2**–**4**. Crystallographic data for compounds **1**–**4** and **6** have been deposited with the Cambridge Crystallographic Data Centre as supplementary publication nos. CCDC-269268 (**1**), -282657 (**2**), -282658 (**3**), -282659 (**4**), and -269269 (**6**). These data can be obtained free of charge at www.ccdc.cam.ac.uk/conts/retrieving.html [or from the CCDC, 12 Union Road, Cambridge CB2 1EZ, UK; Fax: +44-1223-336-033; E-mail: deposit@ccdc.cam.ac.uk]. Thermodiffractometry measurements of the $Cd^{II}$ compound **6** were run under ambient atmosphere in the range $9° < 2\theta < 38°$ with a step size of 0.03° and an acquisition time of 2.5 s per step. The compound was heated to 80 °C with a heating rate of 10 °C $min^{-1}$ and after that diagrams were collected every 5 °C with a heating rate of 1 °C $min^{-1}$ up to 140 °C. Finally, the sample was allowed to cool for 12 h and a new diffraction profile was collected at 30 °C.

**Synthesis of [Cu(μ-ox)(4atr)$_2$]$_n$ (1):** Single crystals of **1** were grown by layering a methanol solution of 4-amino-1,2,4-triazole (0.200 g, 2.5 mmol) onto an aqueous solution of $K_2$[Cu(ox)$_2$]·$2H_2O$ (0.175 g, 0.5 mmol) and $K_2$ox·$H_2O$ (0.061 g, 0.33 mmol). After allowing the solution to stand for 2 weeks, the crystals were isolated in 80% yield by filtration. They were washed with cold water and diethyl ether, and dried in air. $C_6H_8CuN_8O_4$ (319.74): calcd. C 22.54, H 2.52, N 35.05, Cu 19.87; found C 22.48, H 2.52, N 34.99, Cu 19.82. Main IR features (KBr pellet): $\tilde{\nu}$ = 3295 s, 3175 s for ν(N–H); 3115 s for ν(C–H); 1655 vs. for $\nu_{as}(CO_2)$; 1615 s for $\delta(NH_2)$; 1540 m, 1465 m for $\nu_{as}$(C=N); 1360 m, 1310 s for $\nu_s(CO_2)$; 1220 m, 1200 m, 1075 s for $\delta_{ip}$(C–H); 1035 m, 1015 m for $\nu_s$(CO); 970 m for $\delta_{ring}$; 890 m, 850 w $\delta_{op}$(C–H); 800 s for $\delta(CO_2)$; 690 w, 625 s for $\tau_{ring}$; 500 m, 415 m for ν(M–O, M–N) $cm^{-1}$.

**Synthesis of [Ni(μ-ox)(4atr)$_2$]$_n$ (2):** An aqueous solution (10 mL) of 4-amino-1,2,4-triazole (0.168 g, 2.00 mmol) was added dropwise to an aqueous solution (30 mL) containing Ni(ox)·$2H_2O$ (0.080 g, 0.44 mmol) and $K_2$ox·$H_2O$ (0.442 g, 2.4 mmol). Immediately, a green precipitate corresponding to compound **2** appeared. Yield 90%. $C_6H_8N_8NiO_4$ (314.87): calcd. C 22.89, H 2.56, N 35.59, Ni

  

18.64; found C 22.92, H 2.55, N 35.55, Ni 18.62. Main IR features (KBr pellet): $\tilde{\nu}$ = 3305 m, 3215 m for ν(N–H); 3105 m for ν(C–H); 1655 sh for $\nu_{as}(CO_2)$; 1615 vs for $\delta(NH_2)$; 1535 w, 1470 w for $\nu_{as}$(C=N); 1360 m, 1315 m for $\nu_s(CO_2)$; 1230 m, 1205 m, 1070 m for $\delta_{ip}$(C–H); 1020 m for $\nu_s$(CO); 970 m for $\delta_{ring}$; 890 w, 855 w $\delta_{op}$(C–H); 800 m for $\delta(CO_2)$; 685 w, 620 m for $\tau_{ring}$; 490 m, 420 m for ν(M–O, M–N) $cm^{-1}$.

**Synthesis of $[Co(\mu\text{-ox})(4atr)_2]_n$ (3):** The preparation of **3** is analogous to that described for **2** but using $Co(ox)\cdot 2H_2O$ (0.080 g, 0.44 mmol), $K_2ox\cdot H_2O$ (0.737 g, 4.00 mmol) and 4-amino-1,2,4-triazole (0.168 g, 2.0 mmol). A pink polycrystalline powder of **3** was obtained almost immediately. Yield 90%. $C_6H_8CoN_8O_4$ (315.11): calcd. C 22.87, H 2.56, Co 18.70, N 35.56; found C 22.88, H 2.56, Co 18.68, N 35.60. Main IR features (KBr pellet): $\tilde{\nu}$ = 3295 m, 3215 m for ν(N–H); 3105 m for ν(C–H); 1655 sh for $\nu_{as}(CO_2)$; 1615 vs for $\delta(NH_2)$; 1535 m, 1465 w for $\nu_{as}$(C=N); 1365 m, 1320 m for $\nu_s(CO_2)$; 1220 m, 1205 m, 1075 m for $\delta_{ip}$(C–H); 1010 w for $\nu_s$(CO); 965 m for $\delta_{ring}$; 895 m, 855 w $\delta_{op}$(C–H); 800 m for $\delta(CO_2)$; 680 w, 625 m for $\tau_{ring}$; 495 m, 415 m for ν(M–O, M–N) $cm^{-1}$.

**Synthesis of $[Zn(\mu\text{-ox})(4atr)_2]_n$ (4):** 10 mL of a water solution containing $H_2C_2O_4\cdot 2H_2O$ (0.034 g, 0.2 mmol) was added dropwise to an aqueous solution (25 mL) of 4-amino-1,2,4-triazole (0.069 g, 1.00 mmol) and $ZnCl_2$ (0.054 g, 0.40 mmol). Immediately, a white polycrystalline powder of **4** appeared. The precipitate was separated from the mother liquor and it was washed with cold water and diethyl ether, and dried in air. Yield 90%. $C_6H_8N_8O_4Zn$ (321.57): calcd. C 22.41, H 2.51, N 34.85, Zn 20.33; found C 22.43, H 2.52, N 34.82, Zn 20.35. Main IR features (KBr pellet): $\tilde{\nu}$ = 3295 s, 3210 s for ν(N–H); 3100 s for ν(C–H); 1655 sh for $\nu_{as}(CO_2)$; 1615 vs for $\delta(NH_2)$; 1540 m, 1465 m for $\nu_{as}$(C=N); 1370 m, 1320 s for $\nu_s(CO_2)$; 1220 m, 1205 m, 1075 m for $\delta_{ip}$(C–H); 1015 m for $\nu_s$(CO); 970 m for $\delta_{ring}$; 895 m, 850 w for $\delta_{op}$(C–H); 800 s for $\delta(CO_2)$; 685 w, 625 s for $\tau_{ring}$; 500 m, 410 m for ν(M–O, M–N) $cm^{-1}$.

**Synthesis of $[Fe(\mu\text{-ox})(4atr)_2]_n$ (5):** Orange polycrystalline samples of compound **5** were prepared as **4** but using $FeSO_4\cdot 7H_2O$ (0.064 g, 0.2 mmol). Yield 90%. $C_6H_8FeN_8O_4$ (312.02): calcd. C 23.09, H 2.58, N 35.91, Fe 17.90; found C 23.05, H 2.57, N 35.95, Fe 17.96. Main IR features (KBr pellet): $\tilde{\nu}$ = 3340 m, 3300 m, 3215 m for ν(N–H); 3110 m for ν(C–H); 1620 vs for $\delta(NH_2)$; 1530 m, 1460 w for $\nu_{as}$(C=N); 1360 w, 1325 m for $\nu_s(CO_2)$; 1215 m, 1200 m, 1075 m for $\delta_{ip}$(C–H); 1005 m for $\nu_s$(CO); 960 m for $\delta_{ring}$; 885 w, 860 w $\delta_{op}$(C–H); 800 m for $\delta(CO_2)$; 680 w, 620 m for $\tau_{ring}$; 495 m, 410 m for ν(M–O, M–N) $cm^{-1}$.

**Synthesis of $[Cd(\mu\text{-ox})(4atr)_2(H_2O)]_2$ (6):** Prismatic colorless crystals appropriate for the X-ray diffraction were obtained using an analogous method to that described for **2** but using $Cd(ox)\cdot 3H_2O$ (0.072 g, 0.28 mmol), $K_2(ox)\cdot H_2O$ (1.182 g, 5.0 mmol) and 4atr (0.087 g, 1.0 mmol). Yield 60%. $C_6H_{10}CdN_8O_5$ (386.62): calcd. C 18.64, H 2.61, Cd 29.08, N 28.98; found C 18.59, H 2.60, Cd 29.10, N 29.01. Main IR features (KBr pellet): $\tilde{\nu}$ = 3435 s for ν(O–H); 3330 s, 3275 m, 3225 m for ν(N–H); 3130 m, 3105 m for ν(C–H); 1680 m, 1630 sh for $\nu_{as}(CO_2)$; 1610 vs. for $\delta(NH_2)$; 1530 m, 1460 w for $\nu_{as}$(C=N); 1385 w, 1315 m for $\nu_s(CO_2)$; 1200 m, 1070 m for $\delta_{ip}$(C–H); 1005 m, 990 sh for $\nu_s$(CO); 960 w for $\delta_{ring}$; 880 m for $\delta_{op}$(C–H); 790 m for $\delta(CO_2)$; 685 w, 620 m for $\tau_{ring}$; 505 w, 420 w for ν(M–O, M–N) $cm^{-1}$.

**Supporting Information:** XRPD patterns of compounds **2**–**7**. Final Rietveld plots of compounds **3**–**4**. Thermoanalytical (TG/DTA) curves for compounds **1**–**6**. Views of the crystal packing of compound $[Mn(\mu\text{-ox})(4atr)_2]_n$. Magnetostructural parameters for oxalato-bridged nickel(II) compounds.

## Acknowledgments

This work was supported by the Ministerio de Ciencia y Tecnología (MAT2002-03166) and the Universidad del País Vasco/Euskal Herriko Unibertsitatea (9/UPV 00169.310-15329/2003). U. G-C. thanks the latter institution for a predoctoral fellowship.

[1] a) L. Brammer, *Chem. Soc. Rev.* **2004**, *33*, 476–489; b) D. Braga, L. Brammer, N. R. Champness, *Cryst. Eng. Comm.* **2005**, *7*, 1–19.

[2] a) S. L. James, *Chem. Soc. Rev.* **2003**, *32*, 276–288; b) C. Janiak, *Dalton Trans.* **2003**, 2781–2804.

[3] a) B. J. Hollyday, C. A. Mirkin, *Angew. Chem. Int. Ed.* **2001**, *40*, 2022–2043; b) D. Braga, G. R. Desiraju, J. S. Miller, A. G. Orpen, S. L. Price, *CrystEngComm.* **2002**, *4*, 500–509.

[4] a) P. Day, *Supramolecular Engineering of Synthetic Metallic Materials*, Nato Asi Series, vol. C518 (Eds: J. Vecina, C. Rovira, D. B. Amabilino), Kluwer Academic Publishers, Dordrecht, The Netherlands, **1999**; b) M. Verdaguer, *Polyhedron* **2001**, *20*, 1115–1128; c) E. Coronado, P. Day, *Chem. Rev.* **2004**, *104*, 5419–5448.

[5] a) M. Pilkington, S. Decurtins, *Comprehensive Coordination Chemistry II*, vol. 7 (Eds: J. A. McCleverty, T. J. Meyer), Elsevier, University of Berna, Switzerland, **2004**, p. 214–229; b) C. N. R. Rao, S. Natarajan, R. Vaidhyanathan, *Angew. Chem. Int. Ed.* **2004**, *43*, 1466–1496.

[6] a) L. O. Atovmyan, G. V. Shilov, R. N. Lyubovskaya, N. S. Ovanesyan, Y. G. Moronov, S. I. Pirumova, I. G. Gusakovskaya, *JETP Lett.* **1993**, *58*, 818–821; b) S. G. Carling, C. Mathoniere, P. Day, K. M. A. Malik, S. J. Coles, M. B. Hursthouse, *J. Chem. Soc. Dalton Trans.* **1996**, 1839–1843; c) E. Coronado, J. R. Galán-Mascarós, C. J. Gómez-García, J. Ensling, P. Gütlich, *Chem. Eur. J.* **2000**, *6*, 552–563; d) E. Coronado, J. R. Galán-Mascarós, C. J. Goméz-García, V. Laukhin, *Nature* **2000**, *408*, 447–449; e) L. Martin, S. S. Turner, P. Day, P. Guionneau, J. A. K. Howard, D. E. Hibbs, M. E. Light, M. B. Hursthouse, M. Uruichi, K. Yakushi, *Inorg. Chem.* **2001**, *40*, 1363–1371; f) E. Coronado, J. R. Galán-Mascarós, C. J. Gómez-García, E. Martínez-Ferrero, S. van Smaalen, *Inorg. Chem.* **2004**, *43*, 4808–4810.

[7] a) S. Decurtins, H. W. Schmalle, P. Schneuwly, H. R. Oswald, *Inorg. Chem.* **1993**, *32*, 1888–1892; b) S. Decurtins, H. W. Schmalle, R. Pellaux, P. Schneuwly, A. Hauser, *Inorg. Chem.* **1996**, *35*, 1451–1460; c) E. Coronado, J. R. Galán-Mascarós, C. J. Gómez-García, J. M. Martínez-Agudo, *Inorg. Chem.* **2001**, *40*, 113–120; d) R. Andrés, M. Brissard, M. Gruselle, C. Train, J. Vaissermann, B. Malézieux, J.-P. Jamet, M. Verdaguer, *Inorg. Chem.* **2001**, *40*, 4633–4640; e) G. Ballester, E. Coronado, C. Giménez-Saiz, F. M. Romero, *Angew. Chem. Int. Ed.* **2001**, *40*, 792–795.

[8] a) J. Glerup, P. A. Goodson, D. J. Hodgson, K. Michelsen, *Inorg. Chem.* **1995**, *34*, 6255–6264; b) I. Muga, J. M. Gutiérrez-Zorrilla, P. Vitoria, A. Luque, M. Insausti, P. Román, F. Lloret, *Eur. J. Inorg. Chem.* **2000**, 2541–2547; c) H. Xiang, T.-B. Lu, S. Chen, Z.-W. Mao, X.-L. Feng, K.-B. Yu, *Polyhedron* **2001**, *20*, 313–319; d) L. J. Farrugia, S. Lopinski, P. A. Lovatt, R. D. Peacock, *Inorg. Chem.* **2001**, *40*, 558–559; e) F. Tuna, G. I. Pascu, J.-P. Sutter, M. Andruh, S. Golhen, J. Guillevic, H. Pritzkow, *Inorg. Chim. Acta* **2003**, *342*, 131–138.

[9] O. Castillo, A. Luque, P. Román, F. Lloret, M. Julve, *Inorg. Chem.* **2001**, *40*, 5526–5535.

[10] O. Castillo, A. Luque, M. Julve, F. Lloret, P. Román, *Inorg. Chim. Acta* **2001**, *315*, 9–17.

[11] O. Castillo, A. Luque, F. Lloret, P. Román, *Inorg. Chim. Acta* **2001**, *324*, 141–148.

[12] J. P. García-Terán, O. Castillo, A. Luque, U. García-Couceiro, P. Román, F. Lloret, *Inorg. Chem.* **2004**, *43*, 5761–5770.

  

[13] a) J. G. Haasnoot, *Coord. Chem. Rev.* **2000**, *200–202*, 131–185; b) M. H. Klingele, S. Broker, *Coord. Chem. Rev.* **2003**, *241*, 119–132.
[14] a) W. Fitzgerald, J. Foley, D. McSweeney, N. Ray, D. Sheahan, S. Tyagi, *J. Chem. Soc. Dalton Trans.* **1982**, 1117–1121; b) H. Oshio, U. Nagashima, *Inorg. Chem.* **1992**, *31*, 3295–3301.
[15] J. Suárez-Varela, J. M. Domínguez-Vera, E. Colacio, J. C. Avila-Rosón, M. A. Hidalgo, D. Martín-Ramos, *J. Chem. Soc. Dalton Trans.* **1995**, 2143–2146.
[16] C. S. Hong, H. Yoon, Y. S. You, *Inorg. Chem. Commun.* **2005**, *8*, 310–318.
[17] F. H. Allen, *Acta Crystallogr. Sect. B* **2002**, *58*, 380–388.
[18] a) L. Yi, J. Y. Du, S. Liu, X. X. Wang, *J. Chem. Res.* **2004**, 29–31; b) N. V. Podberezskaya, N. V. Pervukhina, V. P. Doronina, *J. Struct. Chem.* **1991**, *32*, 34–39.
[19] G. A. Baker, G. S. Rushbrooke, H. E. Gilbert, *Phys. Rev.* **1964**, *135*, A1272–A1277.
[20] a) J. Cabrero, N. Ben Amor, C. de Graaf, F. Illas, R. Caballol, *J. Phys. Chem. A* **2000**, *104*, 9983–9989; b) J. Cano, P. Alemany, S. Alvarez, M. Verdaguer, E. Ruiz, *Chem. Eur. J.* **1998**, *4*, 476–484; c) S. Alvarez, M. Julve, M. Verdaguer, *Inorg. Chem.* **1990**, *29*, 4500–4507.
[21] a) M. Julve, J. Faus, M. Verdaguer, A. Gleizes, *J. Am. Chem. Soc.* **1984**, *106*, 8306–8308; b) A. Bencini, C. Fabretti, C. Zanchini, P. Zannini, *Inorg. Chem.* **1987**, *26*, 1445–1449; c) A. Gleizes, M. Julve, M. Verdaguer, J. A. Real, J. Faus, X. Solans, *J. Chem. Soc. Dalton Trans.* **1992**, 3209–3216.
[22] Z. Smekal, Z. Travnicek, F. Lloret, J. Marek, *Polyhedron* **1999**, *18*, 2787–2793.
[23] D. Cangussu, H. O. Stumpf, H. Adams, J. A. Thomas, F. Lloret, M. Julve, *Inorg. Chim. Acta* **2005**, *358*, 2292–2302.
[24] E. Coronado, M. C. Giménez, C. J. Gómez-García, F. M. Romero, *Polyhedron* **2003**, *22*, 3115–3122.
[25] M. L. Calatayud, I. Castro, J. Sletten, F. Lloret, M. Julve, *Inorg. Chim. Acta* **2000**, *300–302*, 846–854.
[26] O. Castillo, J. Alonso, U. García-Couceiro, A. Luque, P. Román, *Inorg. Chem. Comm.* **2003**, *6*, 803–806.
[27] a) C. Y. Weng, Ph. D. Thesis, Carnegie Institute of Technology, **1968**; b) A. Meyer, A. Gleizes, J. J. Girerd, M. Verdaguer, O. Kahn, *Inorg. Chem.* **1982**, *21*, 1729–1739.
[28] a) P. Román, C. Guzmán-Miralles, A. Luque, J. I. Beitia, J. Cano, F. Lloret, M. Julve, S. Alvarez, *Inorg. Chem.* **1996**, *35*, 3741–3751; b) A. Escuer, R. Vicente, M. S. El Fallah, J. Jaud, *Inorg. Chim. Acta* **1995**, *232*, 151–156; c) P. Vitoria, I. Muga, J. M. Gutiérrez-Zorrilla, A. Luque, P. Román, L. Lezama, F. J. Zúñiga, J. I. Beitia, *Inorg. Chem.* **2003**, *42*, 960–969.
[29] a) M. E. Lines, *J. Chem. Phys.* **1971**, *55*, 2977–2984; b) G. de Munno, M. Julve, F. Lloret, J. Faus, A. Caneschi, *J. Chem. Soc. Dalton Trans.* **1994**, 1175–1183; c) L.-M. Zheng, X. Fang, K.-H. Lii, X.-Q. Xin, H.-K. Fun, K. Chinnakali, I. A. Razak, *J. Chem. Soc. Dalton Tans.* **1999**, 2311–2316.
[30] a) M. E. Fisher, *J. Math. Phys.* **1963**, *4*, 124–135; b) M. E. Fisher, *Am. J. Phys.* **1964**, *32*, 343.
[31] O. Kahn, *Molecular Magnetism*, VCH, New York, **1993**.
[32] a) M. B. Hursthouse, M. E. Light, D. J. Price, *Angew. Chem. Int. Ed.* **2004**, *43*, 472–475; b) U. García-Couceiro, O. Castillo, A. Luque, G. Beobide, P. Román, *Inorg. Chim. Acta* **2004**, *357*, 339–344.
[33] a) D. Armentano, G. De Munno, F. Lloret, M. Julve, J. Curely, A. M. Babb, J. Y. Lu, *New J. Chem.* **2003**, *27*, 161–165; b) D. J. Price, A. K. Powell, P. T. Wood, *Dalton Trans.* **2003**, 2478–2482.
[34] a) P. Orioli, B. Bruni, M. Di Vaira, L. Messori, F. Piccioli, *Inorg. Chem.* **2002**, *41*, 4312–4314; b) R. A. Prasad, S. Neeraj, R. Vaidhyanathan, S. Natarajan, *J. Solid State Chem.* **2002**, *166*, 128–141; c) S.-Q. Xia, S.-M. Hu, J.-C. Dai, X.-T. Wu, Z.-Y. Fu, J.-J. Zhang, W.-X. Du, *Polyhedron* **2004**, *23*, 1003–1009.
[35] a) S. Petit, G. Coquerel, *Chem. Mater.* **1996**, *8*, 2247–2258; b) O. Castillo, A. Luque, S. Iglesias, P. Vitoria, P. Román, *New J. Chem.* **2000**, *24*, 771–775.
[36] U. García-Couceiro, D. Olea, O. Castillo, A. Luque, P. Román, P. J. de Pablo, J. Gómez-Herrero, F. Zamora, *Inorg. Chem*, in press, **2005**.
[37] a) V. Neil, A. L. Thompson, M. C. Muñoz, A. Galet, A. E. Goeta, J. A. Real, *Angew. Chem. Int. Ed.* **2003**, *42*, 3760–3763; b) C.-H. Lin, S.-L. Wang, *Chem. Mater.* **2002**, *14*, 96–102; c) J. Greve, I. Jeb, C. Näther, *J. Solid State Chem.* **2003**, *175*, 328–340; d) C.-C. Wang, C.-H. Yang, S.-M. Tseng, G.-H. Lee, H.-S. Sheu, K. W. Phyu, *Inorg. Chim. Acta* **2004**, *357*, 3759–3764.
[38] a) H. Remy, *Treatise on Inorganic Chemistry*, VCH, Weinheim, Germany, **1956**; b) S. Kirschner, *Inorganic Synthesis*, vol. 4 (Ed.: E. G. Rochow), McGraw-Hill Book Co., New York, **1960**.
[39] K. Iron, W. Jeitschko, E. Parthe, *LAZY PULVERIX*, Laboratoire de Crystallographie aux Rayons-X, Universtité of Genève, Switzerland, **1977**.
[40] A. Earnshaw, *Introduction to Magnetochemistry*, Academic Press, London, **1968**.
[41] K. Harm, S. Wocadlo, *XCAD*, CAD4 Data Reduction, University of Marburg, Germany, **1995**.
[42] *CrysAlis RED*, version 1.170, Oxford Diffraction, Wroclaw, Poland, **2003**.
[43] A. Altomare, M. Cascarano, C. Giacovazzo, A. Guagliardi, *J. Appl. Crystallogr.* **1993**, *26*, 343–350.
[44] G. M. Sheldrick, *SHELXL93, Program for the Solution of Crystal Structures*, University of Göttingen, Germany, **1993**.
[45] L. J. Farrugia, *WINGX, A Windows Program for Crystal Structure Analysis*, University of Glasgow, Great Bretain, **1998**.
[46] M. Nardelli, *J. Appl. Crystallogr.* **1995**, *28*, 659.
[47] A. L. Spek, *Acta Crystallogr. Sect. A* **1990**, *46*, C34.
[48] J. Rodríguez-Carvajal, *FULLPROF, Program for Rietveld Pattern Matching Analysis of Powder Patterns*, Laboratoire Leon Brillouin, Saclay, France, **1997**.

Received: April 20, 2005
Published Online: September 12, 2005

  